CANADIAN JOURNAL OF EXPLORATION GEOPHYSICS
VOL. 28, NO. 2 (DECEMBER 1992), P. 117-127

PASSIVE SEISMIC MONITORING OF HYDROFRACTURE AND STEAM INJECTION IN HEAVY OIL SANDS NEAR FORT MCMURRAY, ALBERTA

D.J. GENDZWILL[1]

ABSTRACT

Microseismic monitoring was conducted during hydrofracture and steam injection tests of three wells in McMurray Formation heavy oil deposits at Gregoire Lake near Fort McMurray, Alberta. The test was intended to evaluate the microseismic method as a means of monitoring fluid and heat penetration in soft tar sands.

The computer system monitored 16 geophones in 14 m-deep holes located over an area of 3 hectares. The seismic location system was calibrated with dynamite check shots.

No microseismic events were recognized during the hydrofracture of the poorly consolidated sediments, although noise analysis suggests that events with energy equivalent to a small fraction of a gram of explosive would have been detected had they occurred.

Hundreds of microseismic events were recorded and located during five weeks of the steaming process, most of them in the first two days at the tops of the three wells. The shallow events were probably due to thermal effects from the 200° C steam which heated the cold steel casing and cement causing expansion and cracking of the cement.

Seven microseismic events were located at depth, six in the first 11 hours of steam injection. All were near one well at depths above the point of injection, suggesting that steam was lost by moving up through a fracture near the well. The events were probably due to expansion or collapse of steam bubbles.

None of the recorded events appears to be related to the horizontal advance of the thermal front into the McMurray Formation. This is probably due to the unconsolidated condition of the tar sand rock.

INTRODUCTION

In recent years geophysical technology has often been directed to engineering and production projects such as enhanced oil recovery. Laboratory work by Nur and Wang (1987), Tosaya et al. (1987), Wang and Nur (1988) and others has established that physical properties of oil sands change significantly with temperature. Talebi and Cornet (1987), Sarda et al. (1988), Becquey et al. (1989) and others have measured microseismic emissions associated with fluid injection into rock. This report describes monitoring of microseismic activity during enhanced recovery operations in unconsolidated tar sand.

The Gregoire Lake In Situ Steam Project (GLISP) is an experimental project to evaluate hydrofracture and steam injection methods for recovery of heavy oil from the McMurray Formation Cretaceous sands in the Fort McMurray area (Figure 1). Hydrofracture is intended to increase the permeability of rock by forcefully fracturing it with high pressure fluid. Steam injection is intended to decrease the viscosity of crude oil by raising its temperature. Both operations improve the efficiency of recovery of crude oil but some sensing method is useful to detect the pattern of fluid penetration in the subsurface formations. Passive seismic monitoring is one of the methods evaluated for monitoring fluid penetration. Seismic monitoring methods have been successfully used to monitor injection in granite (Baria et al., 1989) but it was not clear whether the method would work in soft Athabasca tar sands.

Seismic activity could be generated in brittle rock if the increase in pore pressure reduces the effective stress in the

Fig. 1. Location map of Gregoire Lake In Situ Steam Pilot project (GLISP).

Manuscript received by the Editor May 16, 1992; revised manuscript received December 2, 1992.

[1]Department of Geological Sciences, University of Saskatchewan, Saskatoon, Saskatchewan S7N 0W0

Funding for this project was provided by Amoco Canada Petroleum Company Ltd., the operator, with partners Petro-Canada and AOSTRA under the Amoco-AOSTRA Gregoire Lake In Situ Pilot Project. Amoco provided a trailer to house instrumentation during the survey. Western Geophysical Corporation of Calgary assisted with the cables and dynamite shots. Amoco, Petro-Canada and AOSTRA have kindly permitted publication of data in this report. Dr. Doug Stead of the University of Saskatchewan reviewed the manuscript and helpful comments were received from anonymous reviewers.

rock, allowing shear failure under an existing stress field, or through tensile splitting of the rock. Steam injection also heats the rock, causing thermal expansion and fractures if the rock is brittle.

Results of Agar et al. (1986, 1987) suggest that brittle failure mechanisms are problematical in Athabasca tar sands. They show that tar sands, with 33 to 42 percent porosity filled with bitumen and water, are essentially cohesionless. Under compression tests, shear failure is controlled by intergranular friction. When heated under constant confining pressure with undrained porosity the pore pressure rises, reducing the effective pressure until the sample loses shear resistance and it fails under low effective stress. Under these conditions, only very small seismic emissions could be expected due to friction between single grains.

Seismic activity could also be generated by phase changes of steam, i.e., bubble formation or collapse. According to Plint and Bosworth (1986), the presence of certain oils promotes drop wise condensation of steam in which there is significantly greater rate of heat transfer than in ordinary film condensation. Steam bubble collapse is known to provide substantial energy. For example, Vaporchoc (TM), a marine seismic source using steam was advertised by CGG in the 1970s.

Three-dimensional (3-D) seismic surveys (Pullin et al., 1987) were also used in an attempt to map steam flood penetration at GLISP. The first 3-D survey conducted prior to any steam injection found buried topographic relief on the McMurray Formation. Repetitions of the 3-D work, after steam injection started, found anomalies that outlined the heated zone. Decreased velocity in the hot rock caused delays and distortion in the reflection data. Wang and Nur (1988) show how increased temperature decreases the viscosity and shear modulus of tars and causes large decreases in seismic speed of tar sands. Three-dimensional surveys also have been used in fire flood enhanced recovery projects where in-situ combustion provides the heat (Greaves and Fulp, 1987).

Borehole-to-borehole seismic tomographic imaging has been used to monitor several enhanced oil recovery projects, incuding both steam and fire flood (Laine, 1987; Macrides et al., 1988; Bregman et al., 1989; and others).

Method

The GLISP site includes a number of wells, steam plant and utilities. The area of the reservoir is covered with muskeg about 10 m deep. A thick gravel pad was laid on the muskeg to provide stability for the test site (Figure 2). Passive seismic monitoring was conducted between October 25 and December 1, 1986. Wells H-4 and H-5 were hydrofractured on October 27. Steaming of wells H-3, H-4 and H-5 commenced October 28.

Instrumentation

A condition of the GLISP project was to use geophones already in place. There were 330 geophones permanently installed for three-dimensional seismic reflection surveys. They were in a rectangular grid spaced 8 m north-south and 16 m east-west, cemented into bedrock below the muskeg in boreholes 14 m deep. The geophones were vertical axis Geosource type SM-11 with 30 Hz resonant frequency, 60 percent damping, and their sensitivity was 30 V/m/s. Only 16 of the geophones were selected for the passive monitoring as shown in Figure 2. At the time of the hydrofracture and steaming there was intense work activity in the middle of the area so the geophones closest to the wells could not be used. Geophone signals were collected by standard seismic cable and brought to the instrumentation trailer for amplification and recording. Fixed gain analog amplifiers were used with 72 dB gain. Filters passed 10 Hz to 200 Hz with a 60-Hz notch.

The monitoring system was designed at the University of Saskatchewan. It consists of software installed on an INTEL Sys310 computer. It includes a 12-bit (72 dB) analog to digital converter, buffer memory, full waveform recording, event picking and interpretation, data plotting and storing. Sample rate was 400 samples per second per channel and 16 channels were monitored.

Event recognition uses a short time average (STA) of the signal and a long time average (LTA). When the STA exceeds the LTA by some ratio, the channel is triggered. STA and LTA times of 0.3 and 3.0 s were used. When

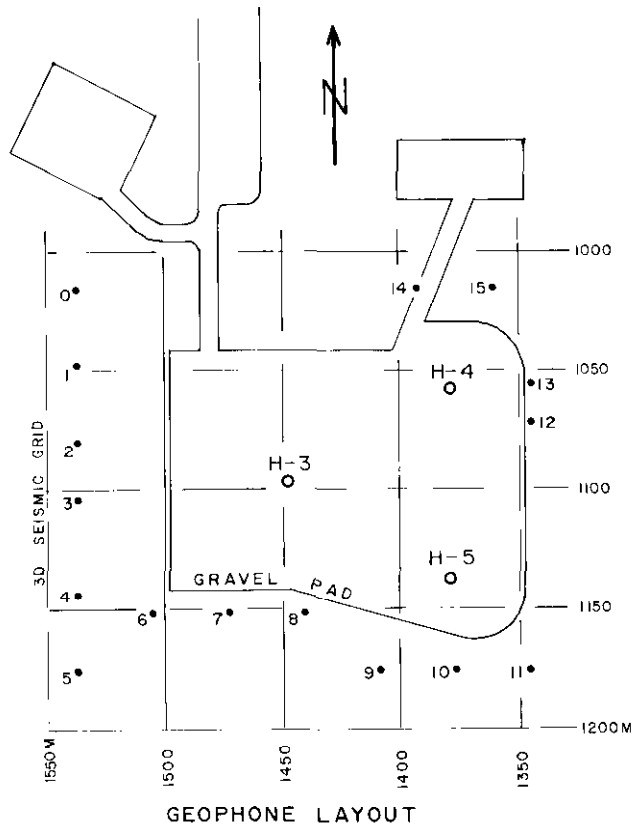

Fig. 2. Site map showing gravel pad, injection wells and geophone locations on the 3-D seismic grid.

several channels are triggered within a time window, an event is declared. Any 4 (usually) of the 16 channels were required to be triggered within 0.2 s in order to declare an event. Two seconds of data were recorded including 0.5 s before and 1.5 s after the trigger.

Source location was done by calculating raypaths and traveltimes through a layered earth from trial source locations to each geophone. Critical and noncritical refractions are allowed. Calculated times from different locations are compared with measured times until a location with a satisfactory time match for all geophones is found. An efficient choice of trial source locations is made by using the simplex algorithm (Prugger and Gendzwill, 1988).

Calibration of the source location algorithm

A horizontally layered earth model was selected based on sonic logs for the area (Figure 3). The low-velocity muskeg layer was not included in the source location calculations because the geophones were located below the muskeg. Two independent calibrations were done, a computed sensitivity test and a field test with explosive check shots.

Sensitivity was calculated for the model by computing traveltimes to each geophone in the array from several assumed source positions near well H-5. The difference in traveltime between the nearest and farthest geophones (moveout) was calculated for the bottom of H-5 and for positions displaced east, north, and up from the bottom of H-5. The difference in moveout time between positions is plotted against the displacement (Figure 4). As shown, a 13.3-m vertical movement of the source caused a change of 2.5 ms (the digitization interval) in moveout. For the north-south and east-west directions the calculated accuracy was somewhat better; 6.4-m and 6.1-m displacement caused 2.5 ms change in moveout.

Ten check shots were made using 18-gram explosive charges. Five of these were in shallow holes at various points in the area. Table 1 shows a comparison of the known and calculated positions of the test shots.

The first attempt in November, 1986, to calibrate with check shots in a deep hole failed because the hole in which the shots had to be fired was dry, and no energy was detected. A second attempt was completed in January, 1987, after the microseismic monitoring equipment had been removed. Data were collected with equipment from a 3-D reflection survey carried out at the time. Five shots were placed at several depths in the well, which then had water in it. Only 16 traces of the 3-D records were selected to match the geophone positions monitored for the microseismic work. The events were picked manually and the regular source location routine used to locate the check shots using the layer model of Figure 3.

Accuracies for the check shot calibrations in the east-west, north-south and vertical directions were respectively 5 m, 4 m and 14 m, comparing favourably with the calculated accuracy estimates, confirming the validity of the model and calculation method.

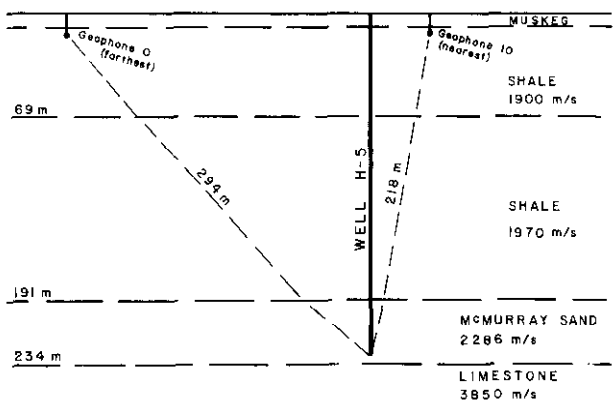

Fig. 3. Layered *P*-velocity structure used for source location, showing nearest and farthest seismic raypaths.

Summary of well treatment

Figure 5 shows a graphical summary of the well treatment during hydrofracture and steaming compared to daily microseismic event counts. Table 2 shows some selected parameters. Hydrofracture of wells H-4 and H-5 occurred on October 27. Steaming of wells H-3, H-4 and H-5 began on October 28. There was a partial to complete loss of steam pressure from November 12 to 16.

At 228 m depth, theoretical hydrostatic pressure is 2.2 MPa but the actual pore pressure may differ somewhat. At 2.2 MPa steam is in liquid phase up to 217° C. The nominal injection temperature was 200° C. Steam at 200° C is in liquid phase at pressures above 1.6 MPa. Hydrostatic pressure is 1.6 MPa at 163 m depth. Therefore, phase changes could occur if the steam escaped to 163 m depth, more or less,

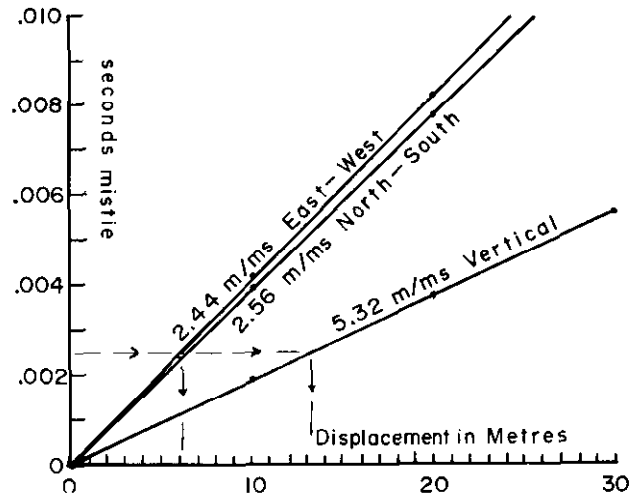

Fig. 4. Calculated calibration for source location sensitivity of geophone array. Vertical axis represents the difference or mistie in moveout time if the source is moved. Horizontal axis represents displacement of a seismic source from the bottom of well H-5. Lines labelled East-West, North-South and Vertical represent the variation in moveout time for the array of geophones as the source position is moved East-West, North-South or Vertical.

Table 1. Measured source location accuracy (metres).

Event	Known Position			Calculated Position			Difference		
	West	South	Depth	West	South	Depth	West	South	Depth
2	1469	1088	18	1469	1090	*	0	+2	
6	1317	1136	18	1306	1145	*	−11	+9	
13	1317	1064	18	1308	1057	*	−9	−7	
18	1541	1136	18	1545	1138	*	+4	+2	
19	1541	1064	18	1546	1063	*	+5	−1	
233	1457	1095	305	1459	1092	322	+2	−3	+17
234	1457	1095	305	1458	1094	317	+1	−1	+12
235	1457	1095	243	1453	1096	229	−4	+1	−14
236	1457	1095	166	1455	1094	145	−2	−1	−21
237	1457	1095	166	1457	1093	166	0	−2	0
	rms error in metres						5.18	3.94	14.47

*Depth fixed for shallow test shots.

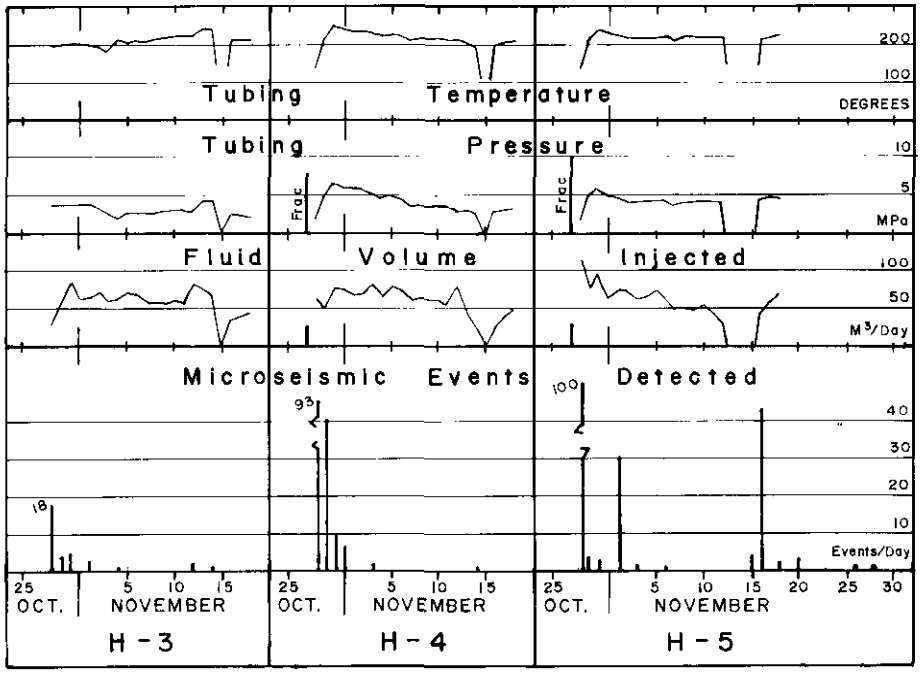

Fig. 5. Treatment history during October 25 to November 18, 1986, for injection wells H-3, H-4 and H-5 and daily microseismic events for October 25 to December 5, 1986.

Table 2. Summary of well treatment.

Well	H-3	H-4	H-5	
Hydrofracture				
Maximum Pressure		8.0	10.2	MPa
Volume Injected		28.3	26.5	m^3
Duration		17	15	minutes
Depth		229	228	metres
Steam Injection				
Initial Temperature	194	140	139	C
Maximum Temperature	200	200	200	C
First-Day Volume	31	65	118	m^3
Total Volume	1231	1270	1242	m^3
Maximum Pressure	4.4	6.9	5.8	MPa
Average Pressur	3.2	3.0	4.0	MPa
Pressure Loss Dates	15	15	13-15	Nov.

depending on the actual pore pressure and if the actual temperature fluctuated above 200° C.

Results

Microseismic events during hydrofracture

Microseismic activity during hydrofracture of the two wells was not detected, neither during injection nor the following day, even though the system was sensitive to very small events.

When the hydrofracture of H-5 began at noon, the system was set to trigger on any four channels. The system turned on numerous times but all the noise was from the trucks and pumps. An example record is shown in Figure 6. Channel 12, the noisiest because it was nearest the trucks, showed about 250 microvolts peak-to-peak amplitude. Channels 0 to 6 on the far side of the pad showed less than 10 microvolts.

The hydrofracture of H-4 began at 18:00. The triggering condition was set to any six channels in order to avoid too many triggers on truck noise and still pick up events from depth which would appear on all channels. Only continuous truck noise was observed, similar to the H-5 data.

Microseismic events detected later during the steaming process had amplitudes ranging from a few tens to several hundred microvolts on all channels with background noise about 2 to 3 microvolts. Similar events, had they occurred during hydrofracture, would have been detected because their amplitudes would have been larger than the noise on most channels (Figure 6).

Microseismic events during steam injection

Microseismic activity began at wells H-5, H-4 and H-3 within minutes after steam injection began in each well. Figure 7 shows the seismic event history for the first few hours. Each well was characterized by a high rate of activity for a time, then the rate decreased to almost zero. The maximum detection rate was 10 records per minute but two or three events from one or more wells frequently appeared on the same two-second record.

Event numbers for each well were different and seemed to be related to the volume of steam injected in each well and to the distance from the well to the nearest geophone (Table 3). Accordingly, an empirical relation was fit to the data by least squares (albeit only three points for the three wells) where E is the event count on the first day, V is the volume in cubic metres of steam injected the first day and D is the distance in metres from the well to the nearest geophone.

$$E = 241 * V/D^{1.5}.$$

Steaming continued during the five weeks of recording. A total of 382 microseismic events were identified and located, mostly near the tops of the three wells. Many other noises were recorded and identified as electrical interference, traffic noise, etc.

Shallow events due to steaming — 375 shallow events were located near the tops of the three wells. The shallow events were characterized by distinctive waveforms consisting of high-frequency first arrivals and second arrivals with larger amplitude and lower frequency. Examples are shown in Figure 8. Seismograms from each well were generally similar and distinct from the other wells. Some events

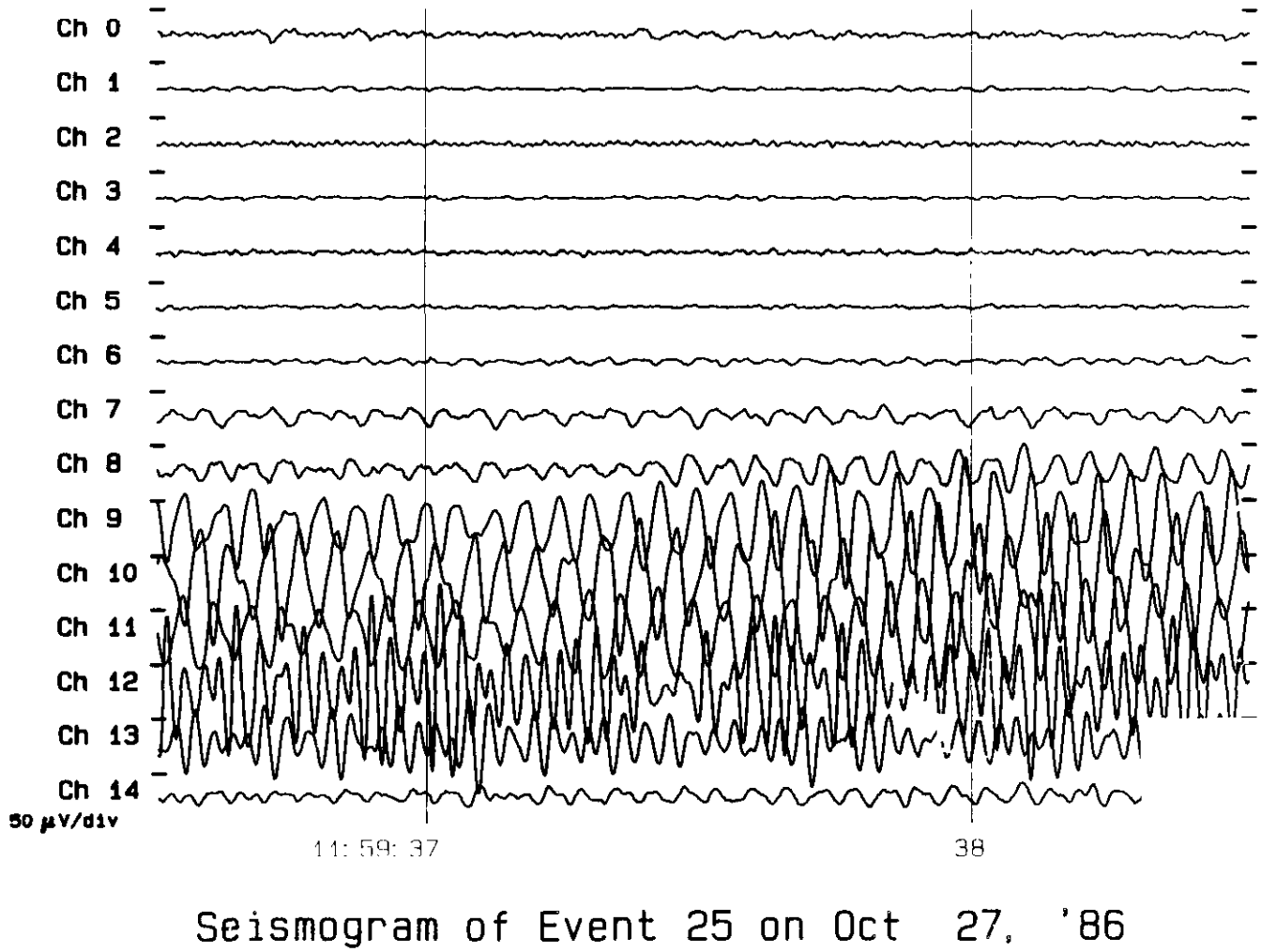

Fig. 6. Example record of truck and pump noise during hydrofracture of H-5, October 27. Record length is two seconds. Vertical trace spacing represents 50 microvolts geophone output.

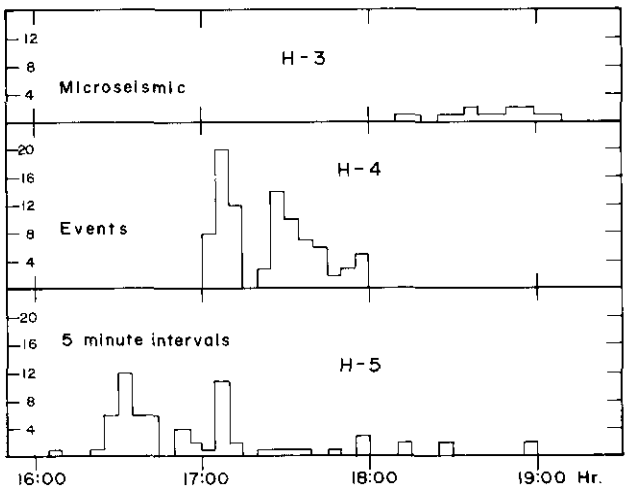

Fig. 7. Histogram of events detected at the start of steaming in the three wells, October 28.

from each well were so similar in amplitude and phase that they were indistinguishable.

The frequency of the first arrivals was 200 Hz or more, aliasing with the 400 samples per second of the recording system. The first arrivals had apparent horizontal velocity of 1900 m/s, the velocity of the top layer in the model (Figure 3). The origins were found to be at one or other of the three wells. These were *P*-waves travelling near the bedrock surface.

Table 3. Event counts, distance and steam volume.

Well		H-3	H-4	H-5
First-Day Event Counts	E	18	93	100
Distance to Nearest Geophone	D in m	56	33	39
First-Day Steam Volume	V in m^3	30.6	64.7	118
Ratio	$(E^*D^{1.5})/V$	246	272	206

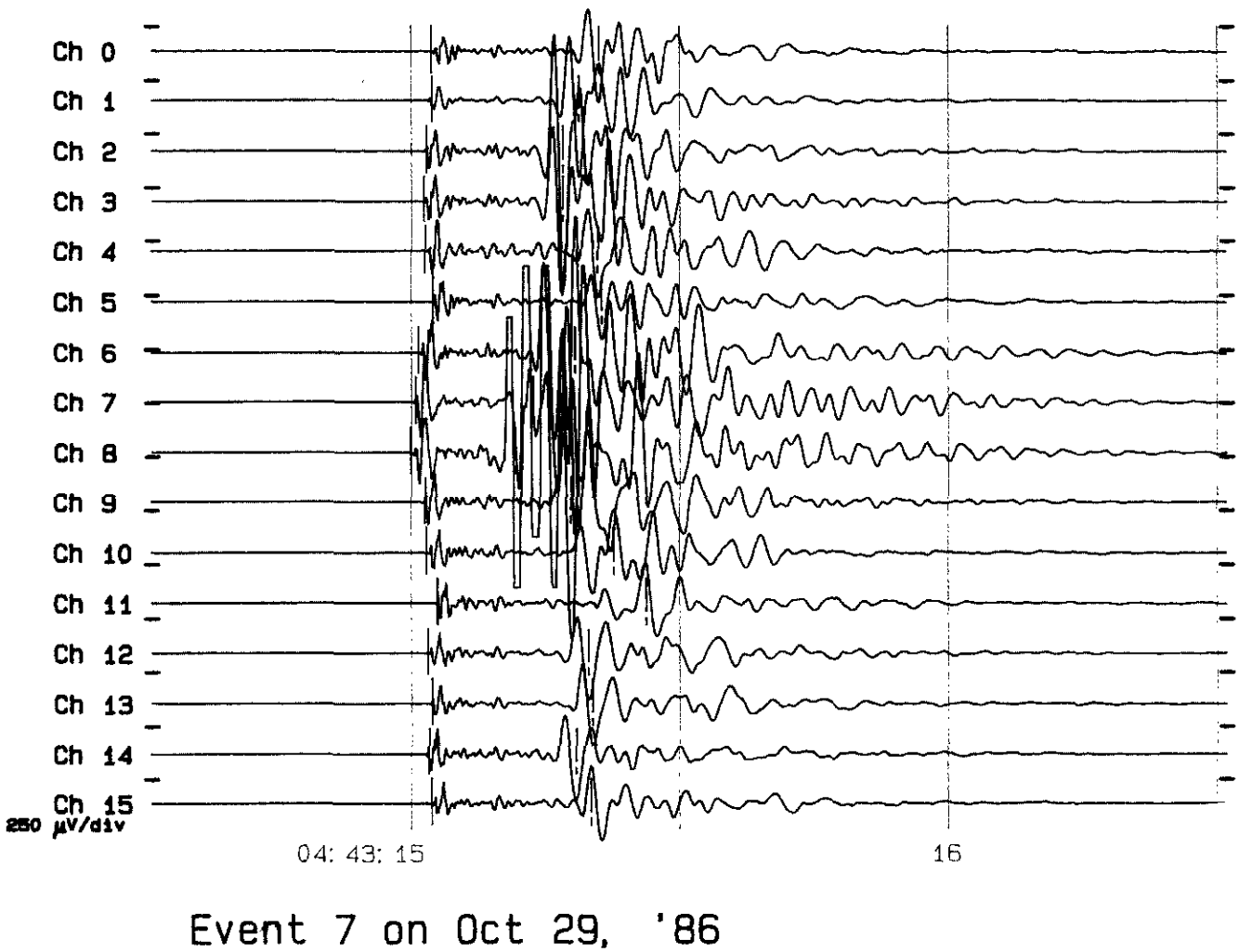

Fig. 8. A shallow event from well H-3. Record length is two seconds. Vertical trace spacing represents 250 microvolts geophone output. Note the large-amplitude surface wave following the *P*-wave.

The amplitude of most first arrivals was less than 50 microvolts but one reached 350 microvolts. In comparison, the amplitude of the dynamite shot was 1700 microvolts, implying that the seismic energy radiated by steam events was very much less than energy radiated by the 18-gram charge.

The frequency of the second arrivals was 30 Hz or less. The amplitude of most second arrivals was approximately 200 to 300 microvolts, although a few were larger. The second arrivals travelled at 300 m/s to 500 m/s. The origin of each second arrival was found to be at the same well as the corresponding first arrival. These were guided surface waves travelling in the muskeg layer.

The shallow events were located close to the surface by the source location algorithm but the algorithm loses precision when the source and the geophones are all located on nearly the same plane. Several other lines of evidence were used to verify the vertical location of the shallow microseismic noises.

The presence of a large surface wave is evidence that the energy was released in or near the surface layer. Events located at greater depth lack the prominent surface wave.

When the shallow (18 m) dynamite calibration shots were taken, a reflection appeared on the seismogram record that could be correlated with the 3-D seismic survey data and with a synthetic seismogram. Some of the seismograms from the larger steam events also showed a reflection, indicating that the depth of the steam event was within 3 m or 4 m of the depth of the dynamite shot because the reflection traveltimes were the same within 2 ms. Figure 9 shows a comparison between a dynamite reflection, a steam reflection and the synthetic seismogram.

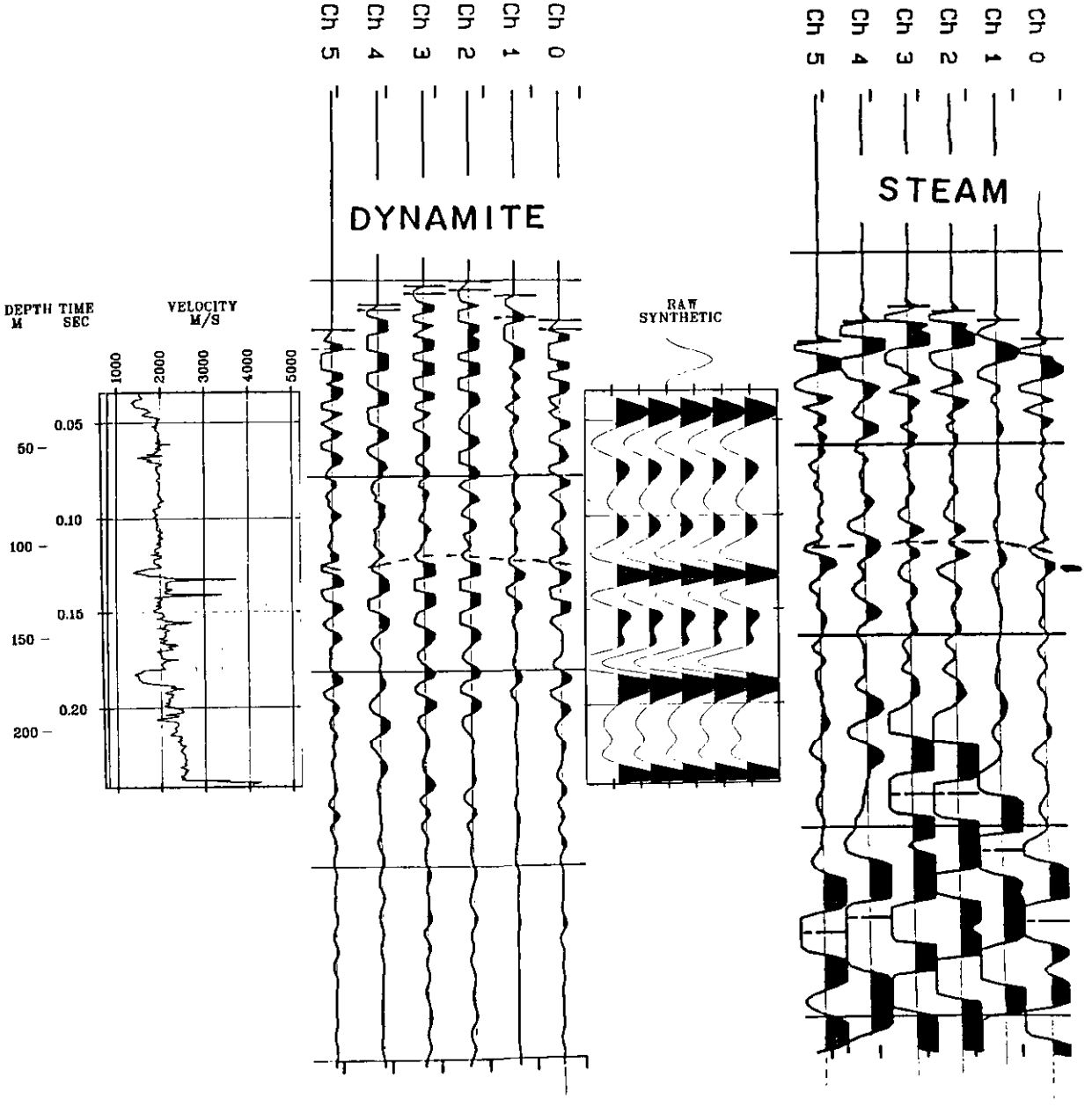

Fig. 9. A comparison of: shallow steam event, dynamite test shot, velocity log and synthetic seismogram. The similar reflection times demonstrate that the microseismic event was located near the surface.

Origin of shallow events — The shallow events occurred at the onset of steaming, October 28, in all wells and at H-5 on November 15 and 16 after a three-day shutdown. They were probably a result of failures of the cement linings due to thermal stress induced by pumping 200° C steam into the cold wells. The thermal coefficient of expansion for both cement and steel is about $12*10^{-6}$ per degree C. The modulus of elasticity for steel is 185 GPa and for concrete it is around 26 GPa. Compressive, shear and tensile strengths for concrete are about 40 MPa, 8 MPa and 3 MPa (Baumeister and Marks, 1967; Eshbach and Souders, 1975). At the onset of steaming, concrete next to the steel pipe may approach 200° C while the concrete in contact with rock may still be cold, setting up a stress differential up to 62 MPa across the thickness of concrete, exceeding its strength. Overburden pressure would compensate the stress differential near the bottom of the well, but not at the top. Similarly, vertical lengthening of the pipe is confined near the bottom but not at the top of the well, inducing shear stress and cracks between the cement lining and the wall rock. When the temperature stabilized after a few hours, the cracking ceased.

Most failures occurred near the top of the pipe. The exact depth would have controlled the details of the wave train so that series of events that were identical would have been generated at the same depth. Events occurring at slightly different depth produced seismograms with slight variations in times and phases of the surface waves and *P*-waves.

Deep events due to steaming — Seven microseismic events were detected and located near the bottom of well H-5, six of them in the first eleven hours (Table 4). No deep events were located near H-3 or H-4. The seven deep events (Figure 10) were easily distinguished from the shallow events. Their dominant frequency was about 50 Hz to 70 Hz. Maximum amplitudes varied from 50 to 630 microvolts, larger than the shallow events. Surface waves were poorly defined and smaller than the first arrivals.

The locations were horizontally clustered in a small group which seems to have a northwest-southeast trend (Figure 11). However, all the horizontal locations could be fit into a circle with radius 4.3 m, less than the horizontal location error of 5 m (Table 1). The centre of the group was 8.8 m east of H-5, a significant distance by the error estimates, so the group of events does not coincide with the well.

The vertical location of the seven events ranged from 169 m to 210 m, a 41-m difference compared to the expected vertical error of 14 m. No microseismic events were located at the injection depth of 228 m.

Origin of the deep events — The first motions of the deep events provide some insight to the source mechanism (Figures 10, 12, Table 4). Polarity was determined by comparison with the dynamite check shots (Table 1). The first six events appear to be implosive sources because the first motion on all geophones was down. The last event on November 28, first motion up on all geophones, could be an explosive type.

An implosive source could have been generated by the rapid collapse of a vapour bubble, perhaps due to cooling and condensation when steam vapour encountered cold water in the porous rock (ambient temperature 7° C). Presumably, porous zones at 200-m and 170-m depth were places where cold water was found by the steam front on the first day.

An explosive steam event might have occurred if high temperature steam came in contact with hot water, causing the water to suddenly flash into steam. This would seem possible if the rock was hot after a long period of steam injection. The explosive-type event on November 28 came after a month of steam injection.

Implosive and explosive steam events could only occur if the temperature was high in the region several tens of metres above the injection point, where pore pressure was low enough to permit phase changes. Favourable conditions would most likely occur where hot steam was transported rapidly upward, for example, through a vertical fracture.

The geometry of the deep events suggests that there was a vertical fracture extending upward from the injection zone. The group of events near 200-m depth coincided with a porous zone into which some of the injected heat escaped as shown in temperature tests conducted in February, 1987. The events at 170- to 180-m depth coincided with another porous zone as shown on the well logs. The porous zones are represented by low-velocity zones in the sonic well log (Figure 9).

H-5 received more steam in the first day (118 m^3) than the other two wells combined (30 m^3 for H-3, 64 m^3 for H-4), which may partly explain why deep microseismic events occurred only at H-5.

The frequency of the deep events, 50 Hz to 70 Hz, was significantly less than the frequency of the shallow events, 200 Hz or more, suggesting different source mechanisms for the deep events and the shallow events.

A shear mechanism for the deep events seems improbable

Table 4. Deep events.

Time Day/Hr:min	Event	Location in m West	South	Depth	Error ms	Amp. microvolt	Motion
Oct 28/18:10	1	1374	1136	200	0.561	50	Down
Oct 28/18:26	2	1370	1139	210	0.784	140	Down
Oct 28/23:11	3	1373	1132	169	0.532	630	Down
Oct 28/23:38	4	1372	1138	184	0.542	390	Down
Oct 28/23:58	5	1376	1135	170	0.791	330	Down
Oct 29/05:10	6	1373	1137	200	0.857	90	Down
Nov 28/18:28	7	1375	1132	180	0.628	80	Up

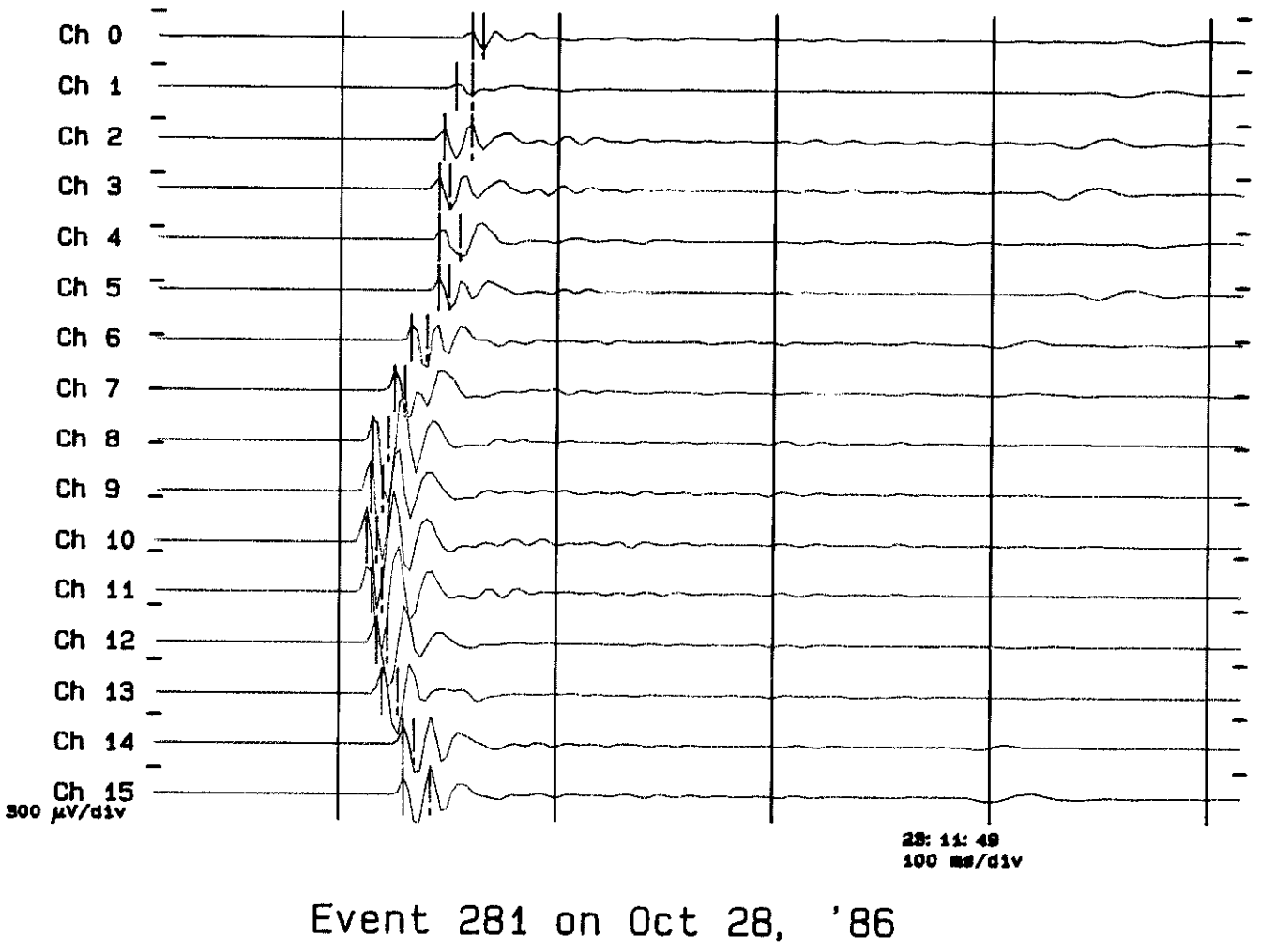

Fig. 10. A deep event from well H-5. Record length is 0.5 seconds. Vertical trace spacing represents 300 microvolts geophone output. Note small surface wave compared to Figure 8 and the relatively large amplitude *P*-wave compared to Figure 6.

because unipolar first motion was observed for all seven events. A shear mechanism requires opposite polarity first motion in different quadrants of the focal sphere but no change in polarity was observed in any single event. A shear mechanism is theoretically possible because the focal sphere was not completely sampled. However, the only possible stress orientation would be with maximum stress axis nearly vertical for the first six events, changing to minimum stress axis vertical for the last event (Figure 12). There is no ready explanation for such consistent orientation of the stress axis nor for a 90-degree rotation at the last event.

Tensile failure of the rock due to injection of high-pressure steam is also inconsistent. Tensile failure would cause outward or upward first motion, whereas downward first motions were observed October 28 and 29. Also, no events were observed during the hydrofracture when pressure was highest.

Discussion

The failure to detect microseismic activity during the hydrofracture of two wells was disappointing but it was consistent with the nonseismic behaviour of tar sands expected on the basis of the results of Agar et al. (1986, 1987). If microseisms are to be detected from cohesionless materials, much more sensitive equipment is needed.

The relatively high microseismic activity during the early stage of the GLISP steaming process was due mostly to thermal effects in the near-surface casing and cement of the wells. Mechanical stress due to the temperature difference caused failure of the cement between the steel lining and the rock. Microseismic monitoring could be a method to detect failure of the cement lining without interfering with the steaming operation.

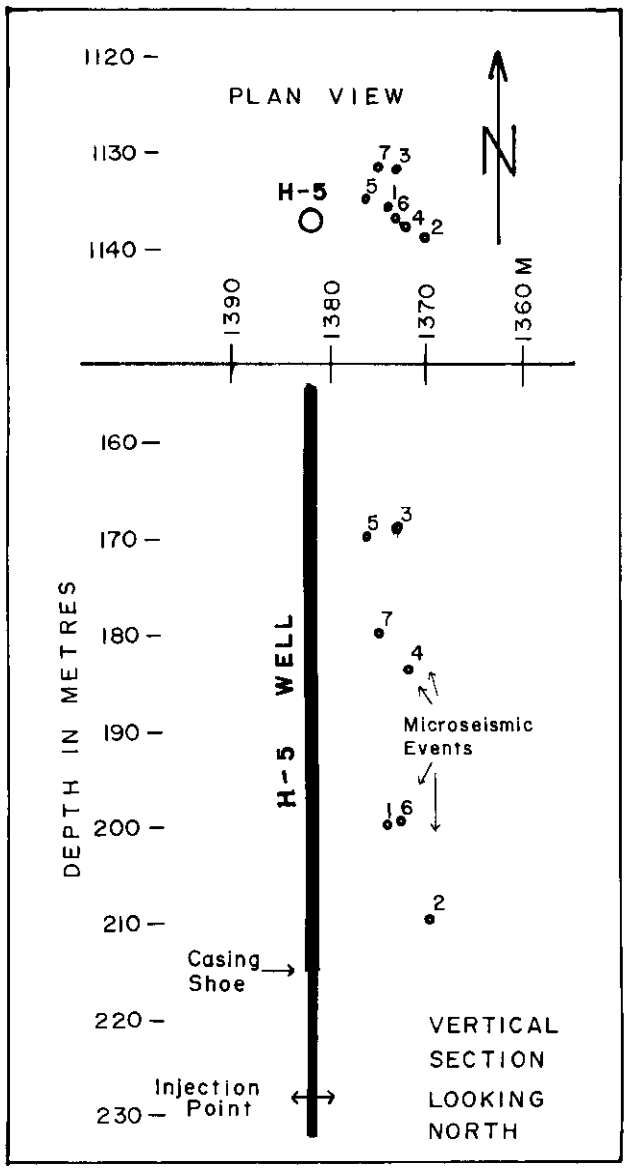

Fig. 11. Location map of deep events from well H-5. Events are numbered in chronological order. In plan view, all events are within one error unit of their mean position. The mean position is more than one error unit from the well axis. In vertical position, the events are separated by more than one error unit. The well diameter is not drawn to scale.

The seven microseismic events that occurred at depth appear to be due to condensation or vaporization effects from the high-temperature steam. Seismic radiation due to elastic failure under thermal stress or external deviatoric stress appears not to have occurred, or was too small to detect, because of the soft nature of the tar sand and because the observed seismic events do not display shear-type failure. The mapped seismic events show where steam may have escaped upward to other porous zones.

Results of this test showed that the monitoring system was very sensitive to microseismic events at 200-m depth. Events were detected whose energy was very small, equivalent

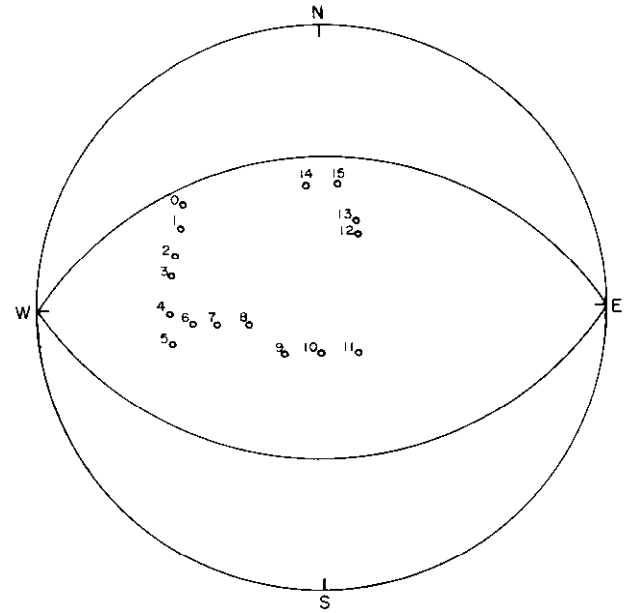

Fig. 12. Source mechanism diagram on the upper hemisphere of a Schmidt net for all deep events. First motions on all geophones for six deep events are all down, suggesting an implosive source mechanism. For the seventh deep event, first motions are all up, suggesting an explosive source mechanism. A shear mechanism is possible but the shear planes would have to fall outside the cluster of points for all events, as shown by the example.

to a small fraction of a gram of explosive. The advantage in this case was the use of multiple geophones in widely separated shallow boreholes, such that at least some of them were in a low-noise environment. One might expect nearly as good sensitivity for greater target depths of monitoring. In more competent rock one might expect also to detect seismic signals from stress failures.

References

Agar, A.G., Morgenstern, N.R. and Scott, J.D., 1986, Thermal expansion and pore pressure generation in oil sands: Can. Geotech. J. **23**, 327-333.

_____, _____ and _____, 1987, Shear strength and stress-strain behaviour of Athabasca oil sand at elevated temperatures and pressures: Can. Geotech. J. **24**, 1-10.

Baria, R., Hearn, K. and Batchelor, A.S., 1989, Induced seismicity during the hydraulic stimulation of the potential hot dry rock geothermal reservoir, *in* Hardy, H.R. Jr., Ed., Fourth conference on acoustic emission/microseismic activity in geological structures and materials: Trans Tech Publ. 327-352.

Baumeister, T. and Marks, L.S., 1967, Standard handbook for mechanical engineers, 7th Ed.: McGraw-Hill Book Co.

Becquey, M., Bernette-Rollande, J.O. and Nicoletis, S., 1989, Microseismicity as a result of fluid injection interruption, *in* Abstracts for the 12th international formation evaluation symposium: The Log Analyst **31**, 33-34.

Bregman, N.D., Hurley, P.A. and West, G.F., 1989, Seismic tomography at a fire flood site: Geophysics **54**, 1082-1090.

Eshbach, O.W. and Souders, M., 1975, Handbook of engineering fundamentals, 3rd Ed.: John Wiley & Sons, Inc.

Greaves, R.J. and Fulp, T.J., 1987, Three dimensional seismic monitoring of an enhanced oil recovery process: Geophysics **52**, 1175-1187.

Laine, E.F., 1987, Remote monitoring of the steam flood enhanced oil recovery process: Geophysics **52**, 1457-1465.

Macrides, C.G., Kanasewich, E.R. and Bharath, S., 1988, Multiborehole seismic imaging in steam injection heavy oil recovery projects: Geophysics **53**, 65-75.

Nur, A.M. and Wang, Z., 1987, In-situ monitoring EOR: the petrophysical basis, *in* SPE annual technical conference and exhibition, general petroleum engineering: Soc. Petr. Eng., Am. Inst. Min. Eng. **62**, 307-314.

Plint, M.A. and Bosworth, L., 1986, Mechanical engineering thermodynamics: a laboratory course: Charles Griffin and Co. Ltd.

Prugger, A. and Gendzwill, D., 1988, Microearthquake location: a nonlinear approach that makes use of a simplex stepping procedure: Bull. Seis. Soc. Am. **78**, 799-815.

Pullin, N.E., Matthews, L. and Hirsche, K., 1987, Techniques applied to obtain very high resolution 3-D seismic imaging at an Athabasca tar sands thermal pilot: Leading Edge **6**, 12, 10-15.

Sarda, J.P., Perreau, P.J. and Deflandre, J.P., 1988, Acoustic emission interpretation for estimating hydraulic fracture extent: laboratory and field analysis, *in* Proceedings, SPE annual technical conference and exhibition: II, production operations and engineering: Soc. Petr. Eng., Am. Inst. Min. Eng., SPE 18192, 113-122.

Talebi, S. and Cornet, F.H., 1987, Analysis of the microseismicity induced by a fluid injection in a granitic rock mass: Geophys. Res. Lett. **14**, 227-230.

Tosaya, C.A., Nur, A.M., Vothanh, D. and Da Prat, G., 1987, Laboratory seismic methods for remote monitoring of thermal EOR: SPE Res. Eng. **2**, 235-242.

Wang, Z. and Nur, A., 1988, Effect of temperature on seismic wave velocities in rocks saturated with hydrocarbons: SPE Res. Eng. **3**, 158.